Quantification of uncertainty in first-principles predicted mechanical properties of solids: Application to solid ion conductors

Zeeshan Ahmad and Venkatasubramanian Viswanathan*
Department of Mechanical Engineering, Carnegie Mellon University, Pittsburgh, Pennsylvania 15213, USA
(Received 1 June 2016; published 16 August 2016)

Computationally-guided material discovery is being increasingly employed using a descriptor-based screening through the calculation of a few properties of interest. A precise understanding of the uncertainty associated with first-principles density functional theory calculated property values is important for the success of descriptor-based screening. The Bayesian error estimation approach has been built in to several recently developed exchange-correlation functionals, which allows an estimate of the uncertainty associated with properties related to the ground state energy, for example, adsorption energies. Here, we propose a robust and computationally efficient method for quantifying uncertainty in mechanical properties, which depend on the derivatives of the energy. The procedure involves calculating energies around the equilibrium cell volume with different strains and fitting the obtained energies to the corresponding energy-strain relationship. At each strain, we use instead of a single energy, an ensemble of energies, giving us an ensemble of fits and thereby, an ensemble of mechanical properties associated with each fit, whose spread can be used to quantify its uncertainty. The generation of ensemble of energies is only a post-processing step involving a perturbation of parameters of the exchange-correlation functional and solving for the energy non-self-consistently. The proposed method is computationally efficient and provides a more robust uncertainty estimate compared to the approach of self-consistent calculations employing several different exchange-correlation functionals. We demonstrate the method by calculating the uncertainty bounds for several materials belonging to different classes and having different structures using the developed method. We show that the calculated uncertainty bounds the property values obtained using three different GGA functionals: PBE, PBEsol, and RPBE. Finally, we apply the approach to calculate the uncertainty associated with the DFT-calculated elastic properties of solid state Li-ion and Na-ion conductors.

DOI: 10.1103/PhysRevB.94.064105

I. INTRODUCTION

Material innovation is at the heart of developing new tools and technologies to address the societal needs for clean energy and human health [1]. First-principles density functional theory (DFT) calculations have played a crucial role in accelerating material innovation by allowing the prediction of chemical [2,3], mechanical [4–6], and electrical [6,7] properties of materials. DFT calculations have been employed to identify new battery electrodes [8], photovoltaics [9], catalysts [10], thermoelectrics [11], etc. An approach to computationally-guided material discovery is to employ a descriptor-based search where materials are screened for a few properties like band gap [12], adsorption energy [13], and HOMO levels [14], and the identified candidates are synthesized, characterized, and tested for their functionality. Given the time and resource consumed for experimental testing and validation, there is a growing realization that it is crucial to quantify the uncertainty associated with the DFT-predicted property values.

The reliability of DFT calculations is typically estimated through comparisons to experiments or to data sets of higher-level calculations [15–17]. Studies using different exchange-correlation functionals have shown considerable variation in properties like adsorption energy [18], structure of liquid water [19], elastic constants [20], vibrational frequencies [21], thermal conductivity [22], infrared spectrum [23], etc. It is therefore of great interest to isolate the error associated with the exchange-correlation functional when comparing DFT-predicted values with experimental values. A recently developed exchange-correlation functional, Bayesian error estimation functional with van der Waals correlation (BEEF-vdW) possesses built-in error estimation capabilities [24]. The Bayesian error estimation [25] within the functional is designed to reproduce known energetic errors by mapping the uncertainties on the exchange-correlation parameters. This capability has been exploited to estimate the uncertainty in adsorption energies and thereby the reliability of calculated catalytic rates for ammonia synthesis [26] and electrocatalytic oxygen reduction [27].

The calculation of uncertainties within the Bayesian error estimation approach has been limited to quantities that are directly related to the ground-state energy [28–31]. In this work, we propose a method to calculate the uncertainty in properties that involve the derivatives of energy, for e.g., mechanical properties. Specifically, we demonstrate the method to estimate the uncertainty associated with the calculated elastic properties for solids. This is done by performing an ensemble of energy-strain fits around equilibrium. The elastic constants for each fit can be calculated in terms of the fitting parameters, and the spread of their distribution can be used to quantify the uncertainty associated with the elastic constants.

We use the developed method to calculate the mechanical properties with uncertainty for candidate solid ion conductors for Li-ion and Na-ion batteries. It has been shown that solid ion conductors that possess a sufficient modulus can suppress the formation of dendrites at the metal anode [32], Here, we focus on four important classes of solid ion conductors: thiophosphate, halide, antiperovskite, and glass. We use the

*venkvis@cmu.edu

ensemble of obtained mechanical property values to determine other properties of interest like the Pugh's modulus ratio with uncertainty bounds.

II. METHODS

A. Property calculation

The elastic constants of a material can be obtained by computing a set of energies for its unit cell at different strains using DFT calculations. The calculated energies can be fit to the energy-strain relationship, and the elastic constants can be extracted from the fitting parameters. There exist several choices for the strains to be applied. We outline the procedure and choices of strains used in this section.

We assume the undeformed coordinates of a point in the material as $\overline{X} = (X_1, X_2, X_3)^T$, where T denotes the transpose. The coordinates are transformed on applying a homogeneous deformation $\overline{\overline{F}}$ such that the new coordinates $\overline{x} = (x_1, x_2, x_3)^T$ are given by $\overline{x} = \overline{\overline{F}}\,\overline{X}$. From the deformation matrix $\overline{\overline{F}}$, we get the Lagrangian strain tensor $\overline{\overline{\eta}}$, given by

$$\overline{\overline{\eta}} = \tfrac{1}{2}(\overline{\overline{F}}^T\overline{\overline{F}} - \overline{\overline{I}}). \tag{1}$$

The energy E of the unit cell having a volume V on applying a Lagrangian strain $\overline{\overline{\eta}}$ can be expressed in terms of the elastic constants C_{ijkl} as

$$E(\overline{\overline{\eta}}) = E_0 + \frac{V}{2}\sum_{ijkl} C_{ijkl}\eta_{ij}\eta_{kl} + O\left(\eta_{ij}^3\right), \tag{2}$$

where E_0 denotes the energy at equilibrium or zero strain. Since all energy calculations in this paper using DFT are performed at 0 K, all elastic constants in Eq. (2) are isothermal constants at 0 K:

$$C_{ijkl}(\text{T=0 K}) = \frac{1}{V}\frac{\partial^2 E}{\partial\eta_{ij}\partial\eta_{kl}}\bigg|_{\overline{\overline{\eta}}=0}. \tag{3}$$

Using the Voigt notation for indices [33] (11 → 1, 22 → 2, 33 → 3, 32 or 23 → 4, 13 or 31 → 5, 12 or 21 → 6), the fourth order elastic tensor can be written in a contracted form as a second order 6×6 tensor. The deformation matrix we choose is of the form $\overline{\overline{F}} = \overline{\overline{I}} + \overline{\overline{\epsilon}}$, where $\overline{\overline{\epsilon}}$ is a symmetric matrix with six independent components [34]:

$$\overline{\overline{\epsilon}} = \begin{bmatrix} e_1 & e_6/2 & e_5/2 \\ e_6/2 & e_2 & e_4/2 \\ e_5/2 & e_4/2 & e_3 \end{bmatrix}. \tag{4}$$

For crystals having cubic symmetry, the elastic tensor has only three independent components: C_{11}, C_{12}, and C_{44}, and only three independent strains are required. On applying a volume-conserving orthorhombic strain [34]

$$\begin{aligned} e_1 &= -e_2 = x, \\ e_3 &= \frac{x^2}{1-x^2}, \\ e_4 &= e_5 = e_6 = 0, \end{aligned} \tag{5}$$

the energy expansion calculated using Eq. (2) is

$$E(x) = E_0 + V(C_{11} - C_{12})x^2 + O(x^4), \tag{6}$$

which can be used to obtain the elastic constant $C_{11} - C_{12}$. Similarly, the energy change due to a volume-conserving monoclinic strain [34]

$$\begin{aligned} e_6 &= x, \quad e_3 = \frac{x^2}{4-x^2}, \\ e_1 &= e_2 = e_4 = e_5 = 0 \end{aligned} \tag{7}$$

can be calculated as

$$E(x) = E_0 + \frac{V}{2}C_{44}x^2 + O(x^4). \tag{8}$$

This gives the elastic constant C_{44}. Further, a uniform strain in all three directions can be used to calculate the bulk modulus $B = (C_{11} + 2C_{12})/3$ and lattice constant by fitting the energies to the Birch-Murnaghan equation of state [35].

For lower symmetry crystals, more strain-energy calculations are required [34,36–38]. Since the only lower symmetry crystal in our calculations has tetragonal symmetry, we show the strains used for this case in Table I.

We used the Voigt-Reuss-Hill approximation [39] to relate the polycrystalline bulk, shear and Young's modulus to the single crystal elastic constants. The Voigt and Reuss approximations for bulk modulus of a cubic polycrystal are the same: $B = (C_{11} + 2C_{12})/2$ whereas the shear modulus is given by [40]

$$G_V = \frac{C_{11} - C_{12}}{5} + \frac{3C_{44}}{5}, \tag{9a}$$

$$G_R = \frac{5(C_{11} - C_{12})}{4C_{44} + 3(C_{11} - C_{12})}. \tag{9b}$$

TABLE I. Strains used determine the elastic constants of crystals with tetragonal symmetry [34].

Strain	Nonzero e_i	Energy change $E(x) - E_0$
1	$e_1 = e_2 = x$	$V(C_{11} + C_{12})x^2 + O(x^3)$
2	$e_1 = e_2 = x$, $e_3 = \frac{-x(2+x)}{(1+x)^2}$	$(C_{11} + C_{12} + 2C_{33} - 4C_{13})x^2 + O(x^3)$
3	$e_3 = x$	$C_{33}x^2/2 + O(x^3)$
4	$e_1 = [(1+x)/(1-x)]^{1/2} - 1$, $e_2 = [(1-x)/(1+x)]^{1/2} - 1$	$(C_{11} - C_{12})x^2 + O(x^4)$
5	$e_4 = e_5 = x, e_3 = x^2/4$	$C_{44}x^2 + O(x^4)$
6	$e_6 = x$, $e_1 = e_2 = (1 + x^2/4)^{1/2} - 1$	$C_{66}x^2/2 + O(x^4)$

The bulk and shear modulus of a tetragonal crystal under the Voigt and Reuss approximations can be calculated using [41]

$$B_V = \frac{1}{9}(2C_{11} + C_{33} + 2C_{12} + 4C_{13}), \tag{10a}$$

$$B_R = \frac{(C_{11} + C_{12})C_{33} - 2C_{13}^2}{C_{11} + C_{12} + 2C_{33} - 4C_{13}}. \tag{10b}$$

$$G_V = \frac{1}{30}[4(C_{11} - C_{13}) + 2(C_{33} - C_{12}) + 6(C_{66} + 2C_{44})], \tag{11a}$$

$$G_R = \frac{30}{4}\left[\frac{2(C_{11} + C_{12}) + C_{33} + 4C_{13}}{(C_{11} + C_{12})C_{33} - 2C_{13}^2} + \frac{3}{C_{11} - C_{12}} + \frac{3}{2C_{66}} + \frac{3}{C_{44}}\right]^{-1}. \tag{11b}$$

The average of the Voigt and Reuss limits was used as the polycrystalline bulk and shear modulus.

$$B = \frac{B_V + B_R}{2}, \tag{12a}$$

$$G = \frac{G_V + G_R}{2}. \tag{12b}$$

The Young's modulus Y and Poisson's ratio ν can be calculated from the bulk and shear modulus using

$$Y = \frac{9BG}{3B + G}, \tag{13}$$

$$\nu = \frac{3B - 2G}{2(3B + G)}. \tag{14}$$

B. Computational details

Self-consistent density functional calculations were performed using the real-space projector-augmented wave (PAW) method [42,43] as implemented in GPAW. [44,45]. The BEEF-vdW exchange-correlation functional [24] with 2000 ensembles was employed for all calculations. A real space grid spacing of 0.14 Å and Monkhorst Pack [46] scheme for sampling the Brillouin zone was used. All calculations were converged to energy <0.1 meV for the unit cell and force <0.01 eV/Å. The k-point density was optimized for individual structures to achieve the desired energy convergence. The strain parameter x was varied between -5 to 5% in steps of 1% or 0.5% in few cases and all energy-strain fittings were performed such that the fitting parameters were converged with respect to the maximum value of x used in the fit. The degree of the polynomial used for fitting was three or four depending on the energy-strain relationship.

C. Bayesian error estimation

The Bayesian error estimation functional with van der Waals correlation (BEEF-vdW) [24] provides a convenient and systematic way of performing realistic error estimates on the energies obtained from DFT calculations within the generalized gradient approximation (GGA). The functional is built upon a combination of the reductionist and empiricist approaches. The exchange enhancement factor $F_x(s)$ in the GGA exchange energy density, $\epsilon_x^{GGA}(n, \nabla n) = \epsilon_x^{LDA} F_x(s[n, \nabla n])$ is given by an expansion in terms of Legendre polynomials B_m [24]

$$F_x^{GGA}(s) = \sum_m a_m B_m[t(s)], \quad t(s) = \frac{2s^2}{4 + s^2}, \tag{15}$$

where a_m are the expansion coefficients which are fitted using training data sets of quantities representing chemistry, solid state physics, surface chemistry, and van der Waals interactions. Overfitting of properties from data sets is avoided by regularization of the GGA exchange expansion. Another parameter in the BEEF-vdW functional α_c arises in the correlation energy E_c which has LDA, PBE, and nonlocal contributions:

$$E_c = \alpha_c E^{LDA-c} + (1 - \alpha_c)E^{PBE-c} + E^{nl-c}. \tag{16}$$

To obtain uncertainty estimates on the DFT predicted energies, an ensemble of functionals around the optimum BEEF-vdW functional is used to calculate the energies non-self-consistently. The ensemble of functionals is generated by creating a probability distribution for the model parameters a_m and α_c such that the spread of the ensemble model predictions on the training data reproduces the errors obtained on using BEEF-vdW self-consistently.

For calculating the elastic constants, we fit the energies to the energy-strain relationship as discussed in Sec. II A. Likewise, propagating uncertainty to the elastic constants would involve performing an ensemble of fits using the ensemble of energies generated at each point. The procedure is illustrated in Fig. 1. The strain type is a uniform strain in

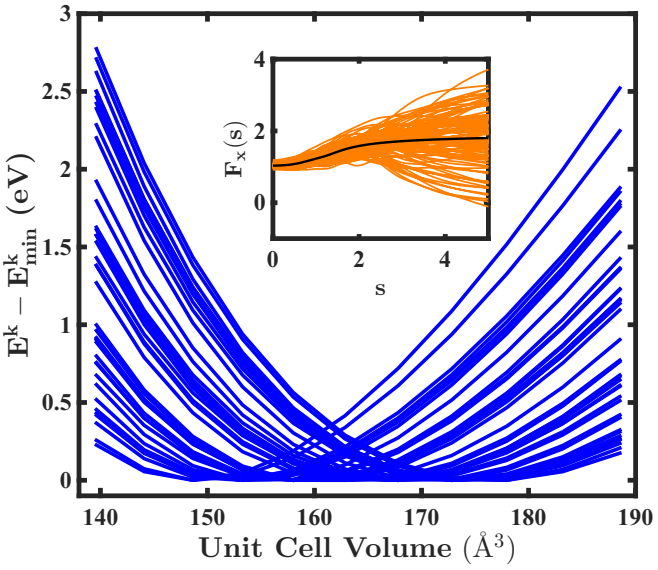

FIG. 1. Ensemble of energy curves for Si obtained on applying a uniform strain in all three directions. The value of unit cell volume at the minima corresponds to the equilibrium volume for that ensemble. The inset shows an ensemble of 100 exchange enhancement factors $F_x(s)$ obtained on perturbing the values of coefficients a_m of the Legendre polynomial B_m in the exchange expansion. The optimum BEEF-vdW exchange enhancement factor is also shown (in dark) for comparison.

all three directions that enables the computation of the unit cell volume and the bulk modulus. From the ensemble of energies generated at different values of the unit cell volume, we can bracket the minima for each such ensemble. This can be used to determine the unit cell volume (or lattice constant) and bulk modulus for the corresponding exchange correlation functional.

The procedure can be summarized as follows:

(1) Choose the values $\zeta = \zeta_1, \zeta_2, \ldots, \zeta_n$ of the independent variable (strain parameter x or unit cell volume V) to be used for fitting. Compute the transformation matrix $\overline{\overline{F}}$ for each case.

(2) Apply the homogeneous transformation $\overline{\overline{F}}$ to the unit cell in each case. Relax the internal coordinates until the force on each atom is lower than the maximum allowed force, and calculate the energy of the relaxed system.

(3) Generate an ensemble of m energies at each ζ using BEEF-vdW and perform the fitting using the relationship between energy and ζ. For the kth ensemble, the fitting can be performed using the array of energies of that ensemble $\overline{\mathfrak{E}}^k = [E^k(\zeta_1), E^k(\zeta_2), \ldots, E^k(\zeta_n)]$.

(4) Calculate the values of the fitting parameters $c_1^k, c_2^k, \ldots c_l^k$ for the kth ensemble using the $E - \zeta$ relationship and use them to calculate the elastic constants for the kth ensemble.

(5) Repeat the process over all m ensembles and generate the ensemble of elastic constants C_{ij}.

It should be noted that the generation of ensembles for the energies and elastic constants is only a post-processing step consuming minimal computation time. The proposed method has a distinct computational advantage over the approach of carrying out self-consistent energy calculations with several exchange-correlation functionals. The values of m and n need to be chosen carefully to get the correct uncertainty estimates. The value of m, the number of ensemble functionals used, should be chosen such that the uncertainty estimate is well converged. The value of n should be chosen such that the values of the fitting parameters are converged and the extreme values of ζ are able to provide a good fit for each of the ensembles, i.e., the minimum falls within the extreme values of ζ. We were able to obtain converged results with $m = 2000$ and $n = 11$ in most cases.

III. RESULTS AND DISCUSSION

We begin by demonstrating our method on different materials belonging to different classes of compounds and having different crystal structures. We then apply our method to a problem of current interest in the battery community.

A. Test cases

In order to test whether our developed method indeed predicts the uncertainty associated with the elastic constants, we performed two sets of calculations for the materials: Si (Group IV), CsCl (Group I-VII compound), cBN (Group III-V compound), and CaS (Group II-VI compound). These materials have different crystal structures defined by their space groups, which are $Fd\bar{3}m$, $Pm\bar{3}m$, $F\bar{4}3m$, and $Fm\bar{3}m$ respectively. Further, the bulk modulus of these materials also encompasses a wide range. First, using our method, we calculated the elastic constants and the associated uncertainty. Second, using a few different GGA exchange-correlation functionals, we calculated the elastic constants. The robustness of the uncertainty estimate is determined by its ability to bound the range of calculated elastic constants. Using BEEF-vdW, we obtained an ensemble of values for each of the elastic constants of the material. As an example, the distribution of values obtained for the elastic constant C_{11} of Si using the developed method is shown in Fig. 2.

Table II shows the values of unit cell volume and the elastic constants of chosen materials calculated using BEEF-vdW and three GGA functionals: PBE [47], PBEsol [48], and RPBE [49]. We used the standard deviation of the distribution of the property values as a measure of the uncertainty. From the table, it is clear that the uncertainty values obtained using the developed method accurately depict the variation in properties due to the choice of exchange-correlation functional. We would also like to emphasize that the uncertainty obtained through the developed method is quite tight in all cases. In most cases, the experimental values also lie within the uncertainty estimates even though the temperature of measurement is generally room temperature.

TABLE II. Equilibrium unit cell volume V (in Å^3) and elastic constants of materials (in GPa) belonging to different classes using our method and different GGA exchange-correlation functionals. The uncertainty estimate used is the standard deviation associated with the elastic constant distribution. The values predicted by different GGA exchange-correlation functionals clearly lie within the uncertainty estimates. The experimental values have also been added for comparison whenever available.

Material	Property	This work	PBE	PBEsol	RPBE	Expt.
Si $Fd\bar{3}m$	V	164.3 ± 6.7	164.2	160.9	167.1	160.2[a]
	B	89.5 ± 9.0	88.7	93.8	94.6	97.9[b]
	C_{11}	155.1 ± 12.9	152.8	156.0	148.5	165.8[b]
	C_{12}	56.7 ± 7.8	56.7	62.7	52.7	63.9[b]
	C_{44}	77.1 ± 4.0	75.8	73.9	75.0	79.6[b]
CsCl $Pm\bar{3}m$	V	79.1 ± 11.6	75.1	67.7	84.6	70.1[c]
	B	13.5 ± 6.1	14.2	17.3	10.3	18.0[d]
	C_{11}	32.2 ± 5.6	32.0	36.1	27.2	36.4[d]
	C_{12}	4.1 ± 6.4	5.4	7.9	1.9	8.8[d]
	C_{44}	5.8 ± 2.9	6.4	9.3	5.6	8.0[d]
cBN $F\bar{4}3m$	V	47.7 ± 1.7	47.6	46.9	48.4	47.3[b]
	B	370.2 ± 70.3	371.9	387.6	359.1	400.0[b]
	C_{11}	781.4 ± 78.3	785.9	818.3	760.4	820.0[b]
	C_{12}	164.6 ± 69.7	164.9	172.2	158.5	190.0[b]
	C_{44}	370.3 ± 21.7	371.0	382.9	391.0	480.0[b]
CaS $Fm\bar{3}m$	V	190.3 ± 8.2	187.2	179.7	194.6	184.2[e]
	B	55.4 ± 5.6	57.1	61.4	52.4	–
	C_{11}	119.3 ± 9.8	123.6	138.3	108.8	–
	C_{12}	23.5 ± 7.7	23.9	23.0	24.2	–
	C_{44}	35.6 ± 3.3	35.4	35.0	35.2	–

[a]Reference [52], 295.7 K.
[b]Reference [52], 298 K.
[c]Reference [50], 298 K.
[d]Reference [51], 298 K.
[e]Reference [53], 294 K.

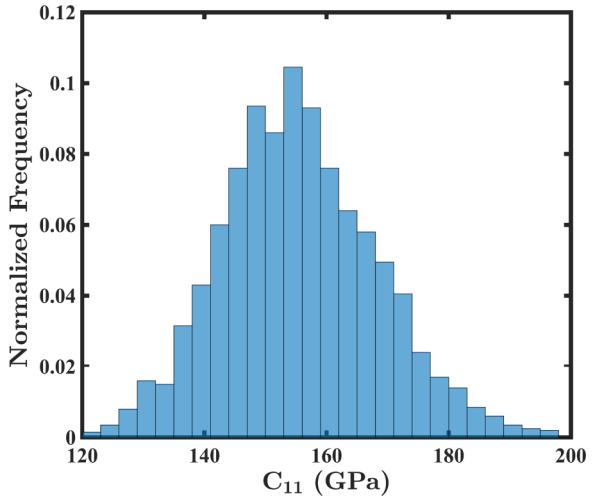

FIG. 2. Distribution of values for the elastic constant C_{11} of Si obtained using our method. The distribution has a standard deviation of 12.9 GPa and is a measure of the uncertainty in C_{11}.

B. Application: Solid ion conductors

Next, we proceed to apply the developed method to the calculation of mechanical properties of solid ion conductors. The mechanical properties of a solid ion conductor used in a Li-ion or Na-ion battery are important for its robust functioning and performance under the strains encountered during cycling. These strains typically arise due to volumetric expansion of the electrodes during intercalation. During such strains, the solid ion conductor should be able to maintain contact with the electrodes without substantial mechanical degradation. Another potential application of a solid ion conductor is to enable Li and Na metal anode by suppressing dendrites at its interface with the electrode. The suppression of dendrites has been linked to the shear modulus of the solid ion conductor. It has been found theoretically that a solid polymer electrolyte with a shear modulus roughly twice that of Li at a Poisson's ratio of 0.33 can suppress Li dendrites [32]. Further, dendritic growth has also been shown to be affected by the Young's modulus of the solid ion conductor [54]. Stress generated at the solid ion conductor due to dendrite growth, higher than the yield strength of Li can result in suppression of Li dendrites through plastic deformation and flattening of the Li metal anode.

We computed the elastic constants of solid ion conductors belonging to four different classes: thiophospahate, antiperovskite, glass, and halide. The results of the calculations are tabulated in Table III.

Most of the property values predicted using BEEF-vdW are in reasonable agreement with previous DFT calculations on solid ion conductors whenever available [20,55]. In many cases, significant uncertainty exists in the elastic moduli due to the exchange-correlation functional. Further, we propagated these uncertainties to a property of interest in solid ion conductors for batteries. The shear modulus is plotted against the bulk modulus in Fig. 3 along with constant Pugh's modulus ratio (G/B) lines. The Pugh's modulus ratio is a measure of the brittleness of the material [56]. Among the solid ion conductors we studied, Li_2S has the highest Pugh's modulus ratio and lies in the brittle regime. However, the uncertainty in the Pugh's modulus ratio predicted from DFT deserves attention due to the nature of the bounds which, in most cases cross the critical Pugh's modulus ratio of 0.571 [56].

Another property of interest for a solid ion conductor is its ability to resist formation of dendrites or smoothen the roughness at the anode due to uneven deposition of Li. We calculated the Poisson's ratio and shear modulus of potential materials for solid ion conductors (Table III) which can be used to determine the dendrite suppressing ability of the material

TABLE III. Calculated elastic constants, bulk, shear, Young's moduli, and Poisson's ratio for different classes of solid ion conductors. The uncertainty estimates used are the standard deviations associated with the distribution.

Material	Volume (Å^3)	C_{ij} (GPa)	B (GPa)	G (GPa)	Y (GPa)	ν
$Li_{10}GeP_2S_{12}$ Thiophosphate ($Li_{10}MP_2S_{12}$) $P4_2mc$	979.8 ± 43.2	C_{11} : 46.5 ± 5.6 C_{12} : 29.6 ± 4.3 C_{13} : 13.6 ± 5.0 C_{33} : 49.5 ± 6.6 C_{44} : 12.1 ± 7.2 C_{66} : 12.5 ± 1.7	28.3 ± 4.4	12.6 ± 3.0	32.8 ± 6.9	0.31 ± 0.05
Na_3PS_4 Thiophosphate (Na-ion) $I\bar{4}3m$	350.9 ± 21.2	C_{11} : 50.2 ± 9.1 C_{12} : 13.3 ± 7.1 C_{44} : 20.9 ± 9.4	25.6 ± 7.5	19.9 ± 4.7	47.4 ± 9.3	0.19 ± 0.10
LiI Halide $Fm\bar{3}m$	220.8 ± 13.2	C_{11} : 33.1 ± 13.7 C_{12} : 15.8 ± 6.3 C_{44} : 16.5 ± 1.7	21.6 ± 5.8	12.8 ± 3.0	32.0 ± 7.2	0.25 ± 0.06
Na_3OCl Antiperovskite $Pm\bar{3}m$	95.6 ± 5.7	C_{11} : 70.0 ± 12.9 C_{12} : 15.2 ± 8.0 C_{44} : 15.8 ± 1.3	33.1 ± 8.5	19.6 ± 2.0	49.0 ± 5.5	0.25 ± 0.07
Li_2S Glass $Fm\bar{3}m$	187.7 ± 12.3	C_{11} : 90.8 ± 14.4 C_{12} : 20.0 ± 12.4 C_{44} : 40.7 ± 3.2	43.6 ± 13.0	38.5 ± 2.0	89.2 ± 8.2	0.16 ± 0.08

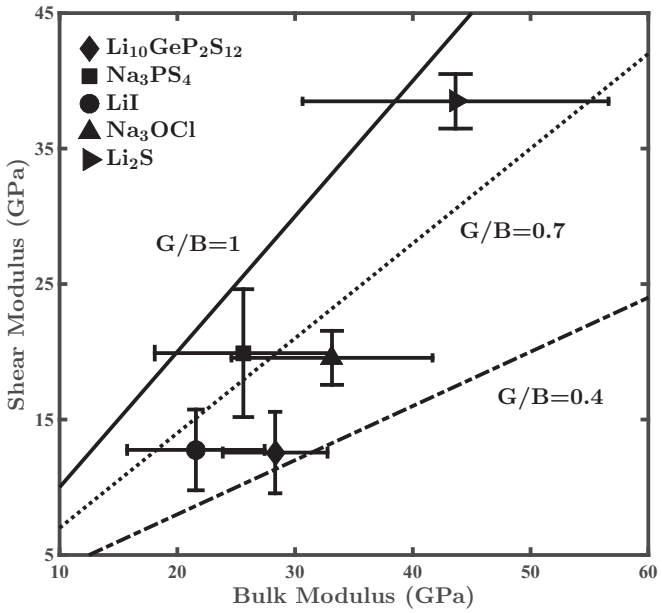

FIG. 3. A plot of shear modulus vs bulk modulus with uncertainties for different solid ion conductors. The straight lines represent points with constant Pugh's modulus ratios.

[32]. We believe that the developed method of quantifying uncertainty will play a crucial role in large scale screening studies for desired mechanical properties. In particular, this method will be critical for the identification of a solid state Li-ion or Na-ion conductor that can mechanically suppress dendrites.

IV. SUMMARY AND CONCLUSIONS

We have developed a method for obtaining uncertainty estimates on the mechanical properties predicted by first-principles calculations. We have demonstrated that the uncertainty estimates obtained through this method capture the variation in property values due to the choice of GGA functional for a range of materials. This allows us to isolate the error in DFT calculations due to the choice of exchange-correlation functional. We applied this method to compute the mechanical properties of different classes of solid ion conductors with uncertainty. The advantage of our method is that different properties of practical interest can be predicted with the confidence that their value will lie within the uncertainty bounds, thereby avoiding multiple self-consistent calculations using several exchange-correlation functionals. We believe that the uncertainty estimation capability will dramatically increase the success of large-scale screening studies for desired mechanical properties.

ACKNOWLEDGMENTS

The authors wish to acknowledge helpful discussions with Alan McGaughey. Acknowledgment is made to the Donors of the American Chemical Society Petroleum Research Fund with PRF# 55009-DNI5 for partial support of this research.

[1] J. Holdren, *Materials Genome Initiative Strategic Plan*, Tech. Rep. (National Science and Technology Council OSTP, Washington, DC, 2014).
[2] W. Kohn, A. D. Becke, and R. G. Parr, J. Phys. Chem. **100**, 12974 (1996).
[3] F. Neese, Coord. Chem. Rev. **253**, 526 (2009).
[4] P. Ravindran, L. Fast, P. A. Korzhavyi, B. Johansson, J. Wills, and O. Eriksson, J. Appl. Phys. **84** 4891 (1998).
[5] R. Astala, S. M. Auerbach, and P. A. Monson, J. Phys. Chem. B **108**, 9208 (2004).
[6] P. J. Hasnip, K. Refson, M. I. J. Probert, J. R. Yates, S. J. Clark, and C. J. Pickard, Phil. Trans. R. Soc. A **372** (2014).
[7] J. Muscat, A. Wander, and N. Harrison, Chem. Phys. Lett. **342**, 397 (2001).
[8] K. Kang, Y. S. Meng, J. Bréger, C. P. Grey, and G. Ceder, Science **311**, 977 (2006).
[9] J. Hachmann, R. Olivares-Amaya, A. Jinich, A. L. Appleton, M. A. Blood-Forsythe, L. R. Seress, C. Roman-Salgado, K. Trepte, S. Atahan-Evrenk, S. Er, S. Shrestha, R. Mondal, A. Sokolov, Z. Bao, and A. Aspuru-Guzik, Energy Environ. Sci. **7**, 698 (2014).
[10] J. K. Nørskov, F. Abild-Pedersen, F. Studt, and T. Bligaard, Proc. Natl. Acad. Sci. USA **108**, 937 (2011).
[11] Y. Tang, Z. M. Gibbs, L. A. Agapito, G. Li, H.-S. Kim, M. B. Nardelli, S. Curtarolo, and G. J. Snyder, Nat. Mater. **14**, 1223 (2015).
[12] I. E. Castelli, T. Olsen, S. Datta, D. D. Landis, S. Dahl, K. S. Thygesen, and K. W. Jacobsen, Energy Environ. Sci. **5**, 5814 (2012).
[13] A. Jackson, V. Viswanathan, A. J. Forman, A. H. Larsen, J. K. Nørskov, and T. F. Jaramillo, ChemElectroChem **1**, 67 (2014).
[14] A. Khetan, H. Pitsch, and V. Viswanathan, J. Phys. Chem. Lett. **5**, 2419 (2014).
[15] K. Lejaeghere, V. V. Speybroeck, G. V. Oost, and S. Cottenier, Crit. Rev. Solid State Mater. Sci. **39**, 1 (2014).
[16] A. M. Teale, O. B. Lutnæs, T. Helgaker, D. J. Tozer, and J. Gauss, J. Chem. Phys. **138**, 024111 (2013).
[17] P. Sałek, T. Helgaker, O. Vahtras, H. Ågren, D. Jonsson, and J. Gauss, Mol. Phys. **103**, 439 (2005).
[18] H. Yildirim, T. Greber, and A. Kara, J. Phys. Chem. C **117**, 20572 (2013).
[19] J. VandeVondele, F. Mohamed, M. Krack, J. Hutter, M. Sprik, and M. Parrinello, J. Chem. Phys. **122**, 014515 (2005).
[20] Z. Deng, Z. Wang, I.-H. Chu, J. Luo, and S. P. Ong, J. Electrochem. Soc. **163**, A67 (2016).
[21] M. De La Pierre, R. Orlando, L. Maschio, K. Doll, P. Ugliengo, and R. Dovesi, J. Comput. Chem. **32**, 1775 (2011).
[22] A. Jain and A. J. McGaughey, Comput. Mater. Sci. **110**, 115 (2015).
[23] L. Maschio, M. Ferrabone, A. Meyer, J. Garza, and R. Dovesi, Chem. Phys. Lett. **501**, 612 (2011).

[24] J. Wellendorff, K. T. Lundgaard, A. Møgelhøj, V. Petzold, D. D. Landis, J. K. Nørskov, T. Bligaard, and K. W. Jacobsen, Phys. Rev. B **85**, 235149 (2012).
[25] J. J. Mortensen, K. Kaasbjerg, S. L. Frederiksen, J. K. Nørskov, J. P. Sethna, and K. W. Jacobsen, Phys. Rev. Lett. **95**, 216401 (2005).
[26] A. J. Medford, J. Wellendorff, A. Vojvodic, F. Studt, F. Abild-Pedersen, K. W. Jacobsen, T. Bligaard, and J. K. Nørskov, Science **345**, 197 (2014).
[27] S. Deshpande, J. R. Kitchin, and V. Viswanathan, ACS Catal. **6**, 5251 (2016).
[28] Y. Wang, J. H. Montoya, C. Tsai, M. S. G. Ahlquist, J. K. Nørskov, and F. Studt, Catal. Lett. **146**, 304 (2016).
[29] R. Christensen, H. A. Hansen, and T. Vegge, Catal. Sci. Technol. **5**, 4946 (2015).
[30] H. Li, C. Tsai, A. L. Koh, L. Cai, A. W. Contryman, A. H. Fragapane, J. Zhao, H. S. Han, H. C. Manoharan, F. Abild-Pedersen, J. K. Norskov, and X. Zheng, Nat. Mater. **15**, 48 (2016).
[31] M. Pandey, A. Vojvodic, K. S. Thygesen, and K. W. Jacobsen, J. Phys. Chem. Lett. **6**, 1577 (2015).
[32] C. Monroe and J. Newman, J. Electrochem. Soc. **152**, A396 (2005).
[33] D. C. Wallace, *Thermodynamics of crystals* (Wiley, New York, 1972).
[34] M. Mehl, B. M. Klein, and A. Papaconstantopoulos, in *Intermetallic Compounds: Principles and Practice*, edited by J. Westbrook and L. Fleischer (John Wiley and Sons, London, 1993).
[35] F. Birch, Phys. Rev. **71**, 809 (1947).
[36] Y. Le Page and P. Saxe, Phys. Rev. B **63**, 174103 (2001).
[37] Y. Le Page and P. Saxe, Phys. Rev. B **65**, 104104 (2002).
[38] J. Zhao, J. M. Winey, and Y. M. Gupta, Phys. Rev. B **75**, 094105 (2007).
[39] R. Hill, Proc. Phys. Soc. Sect. A **65**, 349 (1952).
[40] D. H. Chung and W. R. Buessem, J. Appl. Phys. **38**, 2535 (1967).
[41] P. Sisodia and M. P. Verma, Phys. Status Solidi A **122**, 525 (1990).
[42] P. E. Blöchl, Phys. Rev. B **50**, 17953 (1994).
[43] G. Kresse and D. Joubert, Phys. Rev. B **59**, 1758 (1999).
[44] J. J. Mortensen, L. B. Hansen, and K. W. Jacobsen, Phys. Rev. B **71**, 035109 (2005).
[45] J. Enkovaara, C. Rostgaard, J. J. Mortensen, J. Chen, M. Dułak, L. Ferrighi, J. Gavnholt, C. Glinsvad, V. Haikola, H. Hansen *et al.*, J. Phys.: Condens. Matter **22**, 253202 (2010).
[46] H. J. Monkhorst and J. D. Pack, Phys. Rev. B **13**, 5188 (1976).
[47] J. P. Perdew, K. Burke, and M. Ernzerhof, Phys. Rev. Lett. **77**, 3865 (1996).
[48] J. P. Perdew, A. Ruzsinszky, G. I. Csonka, O. A. Vydrov, G. E. Scuseria, L. A. Constantin, X. Zhou, and K. Burke, Phys. Rev. Lett. **100**, 136406 (2008).
[49] B. Hammer, L. B. Hansen, and J. K. Nørskov, Phys. Rev. B **59**, 7413 (1999).
[50] A. H. Swanson and E. Tatge, Standard X-ray Diffraction Powder Patterns, Natl. Bur. Stand. Ref. Data Ser., Natl. Bur. Stand. (U.S.), Circ. No. 539 (U.S. GPO, Washington, DC, 1953).
[51] H. P. R. Frederikse, in *Handbook of Chemistry and Physics*, 88th ed. edited by D. Lide (CRC Press Taylor and Francis, Boca Raton, 2008).
[52] O. Madelung, *Semiconductors: Data Handbook*, 3rd ed. (Springer, Berlin, 2004).
[53] R. W. G. Wyckoff, *Crystal structures* (Wiley, New York, 1963).
[54] A. Ferrese and J. Newman, J. Electrochem. Soc. **161**, A1350 (2014).
[55] Z. Q. Wang, M. S. Wu, G. Liu, X. L. Lei, B. Xu, and C. Y. Ouyang, Int. J. Electrochem. Sci **9**, 562 (2014).
[56] S. Pugh, Philos. Mag. Ser. 7 **45**, 823 (1954).